Smart Materials and Structures

LETTER

Enhancing magnetorheological effect using bimodal suspensions in the single-multidomain limit

To cite this article: José R Morillas *et al* 2018 *Smart Mater. Struct.* **27** 07LT01

Letters
IOP Publishing
Smart Materials and Structures
Smart Mater. Struct. 27 (2018) 07LT01 (7pp)
https://doi.org/10.1088/1361-665X/aac8ae

Letter

Enhancing magnetorheological effect using bimodal suspensions in the single-multidomain limit

José R Morillas[1], Antonio J F Bombard[2] and Juan de Vicente[1]

[1] Biocolloid and Fluid Physics Group and Excellence Research Unit 'Modeling Nature' (MNat), Department of Applied Physics, Faculty of Sciences, University of Granada, C/Fuentenueva s/n, E-18071—Granada, Spain
[2] Universidade Federal de Itajubá, ICE/DFQ, Av BPS 1303, Itajubá/MG, Brazil

E-mail: jvicente@ugr.es

Received 3 April 2018, revised 9 May 2018
Accepted for publication 30 May 2018
Published 8 June 2018

Abstract

We demonstrate a new route to enhance the magnetorheological effect using bimodal suspensions in the single-multidomain limit. Experimental results are satisfactorily compared to 3D finite element method simulations. The physical reason behind this enhancement is the coating of the larger particles by the smaller ones due to the remnant magnetization of the latter.

Keywords: magnetorheology, magnetorheological fluids, bidisperse, yield stress, MR fluids, nanoparticles, composites

(Some figures may appear in colour only in the online journal)

Introduction

Bimodal suspensions are particle mixtures having two well-differentiated size distributions. In the following, we will call σ_L to the mean particle diameter of the large size distribution and σ_S to the mean particle diameter of the small size distribution.

At present, bimodal suspensions constitute a widely used approach to enhance magnetorheological (MR) effect or to minimize sedimentation. In general, for the MR effect to be sufficiently large, the largest particles in suspension must be in the range $\sigma_L \approx 10\,\mu$m [1]; otherwise Brownian motion disrupts the field-induced structures. With this in mind, previous works in this field can be classified in two limiting cases; either $\sigma_L/\sigma_S \approx 10$ [2–11] or $\sigma_L/\sigma_S \approx 1000$ [12–17].

For $\sigma_L/\sigma_S \approx 10$, experimental and simulation works demonstrate an on-state yield stress enhancement if compared to monomodal suspensions composed of either the small or large particles. Contrary to the intuition, particle level simulations suggest that the reason for this enhancement is not associated with an increase in particle packing within the aggregates but to the changes bimodality causes in the microstructure [7, 10]. These bimodal suspensions suffer from important sedimentation problems because of the large particle sizes.

For $\sigma_L/\sigma_S \approx 1000$, experiments demonstrate that sedimentation is strongly mitigated because of the thermal convection of the nanoparticles that delay the sedimentation of the bigger ones. The price to be paid is that the on-state yield stress is substantially reduced (when the concentration of the small particles exceeds approx. 10 wt%) presumably because of chain growth inhibition or inferior magnetic properties of the nanoparticles if compared to the microparticles [15].

In this letter we demonstrate that bimodal suspensions in the frontier (i.e. $\sigma_L/\sigma_S \approx 100$) exhibit a significantly larger on-state yield stress if compared to their monomodal counterparts and at the same time sedimentation is significantly reduced. The explanation for this is that the smallest particles in the formulation have a size in the range between magnetic mono- and multidomains and therefore exhibit a remarkable remnant magnetization [18]. Because of this, the smallest particles surround the bigger ones increasing the on-state response and reducing the sedimentation. Finite element method calculations qualitatively explain the experimental observations.

Experimental

Both kinds of particles used in the formulation of the bimodal MR fluids were made of iron. The biggest ones ('Large particles') were a gift from BASF SE (EW grade, Germany). The smallest particles ('Small particles') were obtained from US Research Nanomaterials (Iron Nanopowder/Nanoparticles; Fe, 99.5 +%, 95–105 nm, metal basis). SEM observations were carried out to determine their morphological characteristics while squid magnetometry was used to determine the magnetic characteristics of the particles (see table 1). As observed, the magnetic properties are slightly superior for small particles at low fields (i.e. larger initial permeability); the contrary is true for large fields (i.e. smaller saturation magnetization).

The particles were thoroughly dispersed at various mixing ratios in polyalphaolefin oil (PAO 2 cSt, dynamic viscosity 6.4 mPa s, Synfluid, Chevron-Philips). To facilitate the processability of the MR fluids, a certain amount of 1-octanol was also added to the PAO (3.5 wt% in the total amount of PAO) [19].

Steady shear rheometry was carried out in a rotational rheometer (MCR 501, Anton Paar). Magnetic fields were generated using a MRD70/1T magnetocell in parallel plate configuration (20 mm diameter, 300 μm gap). Yield stresses were obtained using a carefully designed protocol. This protocol consisted in several stages: Stage (1) a constant rim shear rate ($\dot{\gamma} = 100\,\mathrm{s}^{-1}$) was applied during 20 s. Stage (2) the upper plate was stopped and a uniaxial DC magnetic field ($147\,\mathrm{kA\,m}^{-1}$) was suddenly applied for 60 s to structure the MR fluid. Stage (3) a stress log-ramp was imposed to evaluate the yielding point similarly to [20]. The interval time employed to get every data within the full rheogram was 5 s. At least three independent measurements with fresh new samples were taken. Error bars in the figures correspond to the standard deviation of the different repetitions.

To explore the sedimentation stability (in the absence of fields) a given volume of MR fluid was placed inside a cylindrical plastic tube and visually observed during time to determine the time evolution of sedimentation ratio $H(t)/H_0$ curves. Here $H(t)$ represents the height of the sediment/liquid interface (i.e. mudline) at a given time, t, and H_0 is the corresponding height value of the MR fluid at the beginning of the test $H_0 \equiv H(t = 0)$.

Penetration and redispersibility tests were carried out using a four-blade vane tool attached to the MCR 501 rheometer head coupling. The test consisted in slowly displacing the tool ($1\,\mathrm{mm\,s}^{-1}$) towards a fully sedimented suspension (i.e. one week after preparation) while recording the axial (normal) force acting on the vane. Once the vane was well inside the sample, a continuous torque ramp was initiated to determine the flow curve (from 0.0001 to 0.5 mN m).

Simulations

3D finite element method simulations were also carried out to compute the on-state yield stress in bimodal MR fluids. For this, the largest particles in the ensemble were arranged in a cubic network of infinite single particle-width chains aligned in the direction of the external magnetic field. Two possibilities were explored with regards to the spatial distribution of the smallest particles in the suspension under the presence of magnetic fields (see figure 1).

Case 1. On the one hand, due to their non-negligible remnant magnetization, the smallest particles could stick around the larger ones covering them with a layer of thickness d_S (i.e. *core–shell* supraparticles). The magnetic properties of the *shell* are therefore dictated by the magnetic properties of the smallest particles.

Case 2. On the other hand, due to their nanometric size, the smallest particles could remain properly dispersed within the carrier liquid, because of thermal/Brownian motion, hosting the largest particles. The magnetic properties of the *carrier fluid* are therefore given by the magnetic properties of the suspension of small particles (with volume concentration ϕ).

The magnetic field distribution was computed in the magnetostatic limit, without free currents, using COMSOL Multiphysics software. A reduced field formulation was employed to split the total magnetic field $\vec{H}$ into the external applied field $\vec{H}_{\mathrm{ext}}$ and the perturbation due to the magnetic suspension $\vec{H}_{\mathrm{p}} = -\overrightarrow{\nabla V_p}$. An important advantage of using the reduced field formulation is that it is not necessary to fix the magnetic field in any boundary of the computational domain and therefore the deformation of a unit cell is representative of the full lattice with periodic boundaries [21]. The dimensions of the unit cell (B_h, B_w) are a function of the large particle diameter σ_L, and the concentration of small ϕ_S and/or large ϕ_L particles (see figure 1). Two scenarios were studied.

Case 1. In the first case, it is supposed that all small particles stick to the larger ones. Therefore, the thickness of the shell is given by $d_S = \sigma_L(1/\sqrt[3]{8(1-\phi_r)} - 1/2)$ where $\phi_r \equiv \phi_S/\phi_T$ and $\phi_T \equiv \phi_S + \phi_L$. As a result, $B_h = \sigma_L + 2d_S$ and $B_w = \sqrt{\pi(\sigma_L + 2d_S)^2/6\phi_T}$ in order to fulfill the condition that the magnetic concentration inside the cell is ϕ_T.

Case 2. In the second case, as the small particles are supposed to remain suspended within the continuum phase, cell dimensions only depend on ϕ_L and on the diameter of the bare large particles σ_L: $B_h = \sigma_L$, $B_w = \sqrt{\pi\sigma_L^2/6\phi_L}$.

The nonlinear magnetic behavior of both populations of particles was accounted for by means of Fröhlich–Kennelly equation using experimental fitting parameters from the powders; initial permeability and saturation magnetization [22]. The magnetic properties of the suspensions of small particles were calculated using Maxwell-Garnett theory [23]. Assuming that all small particles inside the unit cell constitute a suspension, the relationship between the small particles concentration ϕ_S and the suspension concentration ϕ is given by:

$$\phi = \frac{\phi_s B_h B_w^2}{B_h B_w^2 - \pi\sigma_L^3/6} = \frac{\phi_s}{1-\phi_L}. \quad (1)$$

Table 1. Iron powders used in the formulation of the bimodal MR fluids. 'Large' stands for the carbonyl iron microparticles and 'Small' stands for the iron nanoparticles. *N* stands for the number of particles counted to evaluate the particle size.

Particles	Number average diameter (nm)	Weight average diameter (nm)	Volume average diameter (nm)	Polydispersity index (−)	Initial magnetic permeability (−)	Coercive field, H_C ($A\ m^{-1}$)	Saturation magnetization, M_S ($emu\ g^{-1}$)	*N* (−)
Large	1327.4	2642.8	1729.3	1.991	7.42	0.7	204	446
Small	111.64	206.99	137.87	1.854	9.66	11	176	286

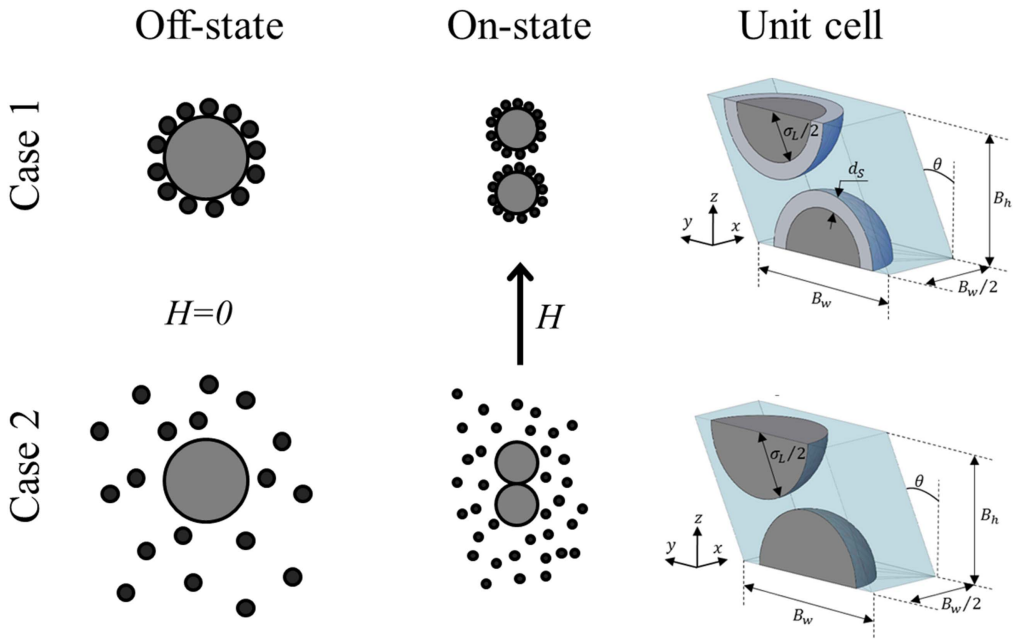

Figure 1. Two cases are considered for small iron particles. In the first one they are adhered to large iron particles due to their remnant magnetization. In the second case, small particles are well dispersed in suspension. Both cases were modeled in the on-state using FEM simulations. A schematics of the computational domain is also represented: a strain $\gamma = \tan\theta$ is applied in the y direction while the magnetic field is applied in the z direction. Periodic boundary conditions are fixed in all boundary faces except in those faces perpendicular to x direction, where mirror symmetry boundary conditions apply.

Once the magnetic field distribution is computed within the computational domain, the shear stress τ on the lower half of the lattice is calculated similarly to [21, 24] by integrating the Maxwell stress tensor on the plane (normal to the external field direction) that halves the unit cell:

$$\tau = \frac{2\mu_0}{B_w^2}\int H_y H_z \,\mathrm{d}S. \tag{2}$$

Finally, the static yield stress τ_y is given by the maximum shear stress achieved as the strain level is increased. It is worth to remark that the affine deformation experienced by the cubic lattice under a simple shear flow is simply modeled here by shearing its unit cell (see figure 1). Due to the symmetries of the sheared cubic lattice, the computational domain can be reduced to one half of the unit cell.

Results and discussion

Figure 2(a) shows the results for the on-state yield stress, at a fixed large particles concentration of $\phi_L = 0.30$, as a function of the concentration of small particles ϕ_S. As observed, the yield stress increases upon increasing the concentration of small particles. This was expected because the total iron concentration $\phi_T \equiv \phi_S + \phi_L$ is increasing. Interestingly, numerical simulations predict reasonably well the order of magnitude for the yield stress despite the simplifications in the model. Note that there are not free fitting parameters. Only in the case where the nanoparticles are coating the microparticles (case 1), the yield stress increases with ϕ_S in good qualitative agreement with the experimental results. Numerical simulations for microparticles dispersed in suspensions of small particles give a yield stress that monotonically decreases with ϕ_S in good agreement with previous experimental data reported in the literature for $\sigma_L/\sigma_S \approx 1000$ [15]. The fact that the experimental yield stress increases faster than the numerical simulations for core–shell particles is expected because of the simplification in the microstructure. In practice the shell should be porous and asymmetric in the field direction (see figure 3).

In figure 2(b) we show the on-state yield stress as a function of the relative concentration of small particles ϕ_S/ϕ_T for a constant total concentration $\phi_T = 0.45$. In this case the addition of small particles results in a significant increase in the yield stress: approximately, a twofold increase is obtained when 5% of the large size particles are replaced by smaller ones (see second experimental data point in figure 2(b); $\phi_S/\phi_T = 11\%$). The reason of this enhancement is presumably again the formation of a shell of small particles surrounding the larger ones (see below). This hypothesis is supported by simulation results although the increasing rate is clearly smaller than in the experimental case. Figure 2(b) also demonstrates that the hypothesis that nanoparticles remain well dispersed within the carrier fluid is not realistic; in this case the simulated yield stress decreases with ϕ_S in contrast to experiments.

To get a better understanding of the internal structure of the aggregates we also performed microscopy observations. In figure 3 we show scanning electron microscopy pictures of the micro and nanoparticles within a resin after gelation under DC magnetic fields (750 mT). As observed, the larger

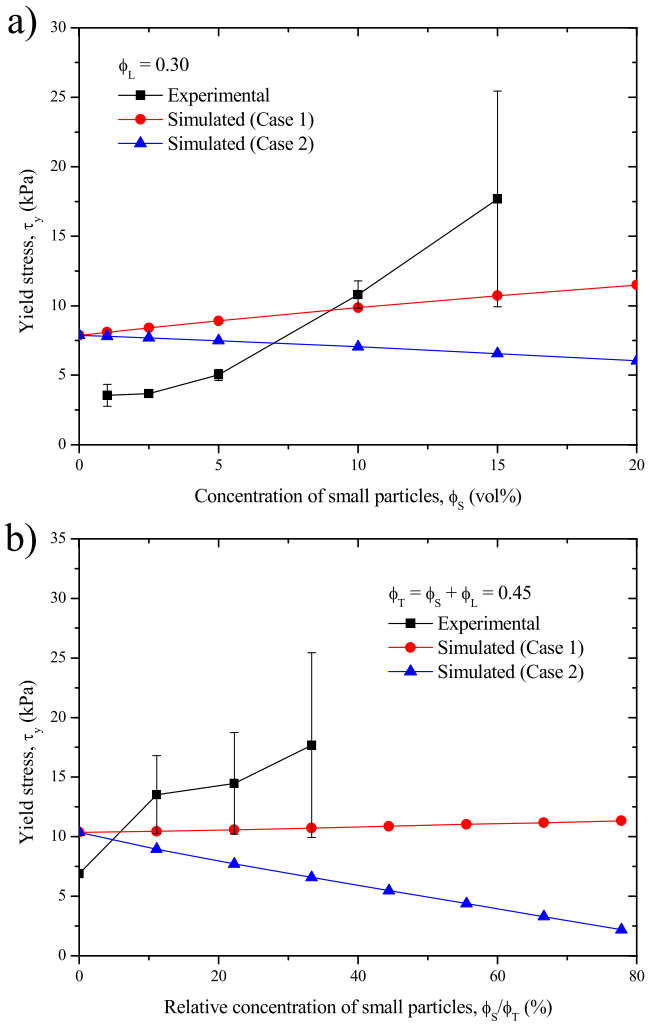

Figure 2. On-state yield stress of bimodal MR fluids as a function of: (a) concentration of small particles ϕ_S for a constant volume fraction of large iron particles of 30 vol% ($\phi_L = 0.30$); (b) fraction of small particles ϕ_S/ϕ_T for a constant total volume fraction of solids of 45 vol% ($\phi_T = 0.45$). The external magnetic field strength is 147 kA m^{-1}.

particles are clearly surrounded by a shell of nanoparticles in good agreement with our hypothesis.

A useful way to visualize the importance of adding a second population of nanoparticles to the suspension of large particles is through the so-called effective enhancement, that is defined as follows:

$$[\tau_{yb}(\phi_S + \phi_L = 0.45) - \tau_{ym}(\phi_L = 0.45)]/\tau_{ym}(\phi_L = 0.45). \quad (3)$$

The effective enhancement directly compares the performance of bimodal suspensions τ_{yb} to monomodal ones τ_{ym} having the same total concentration $\phi_T \equiv \phi_S + \phi_L = 0.45$. Results are contained in figure 4. Here we clearly observe a remarkable increase in the effective enhancement for bimodal MR fluids containing small particles in striking contrast to monomodal MR fluids only containing large particles. Simulations considering core–shell supraparticles also show an enhancement of the yield stress although its increase is not so significant. Again, the fact that the order of magnitude is

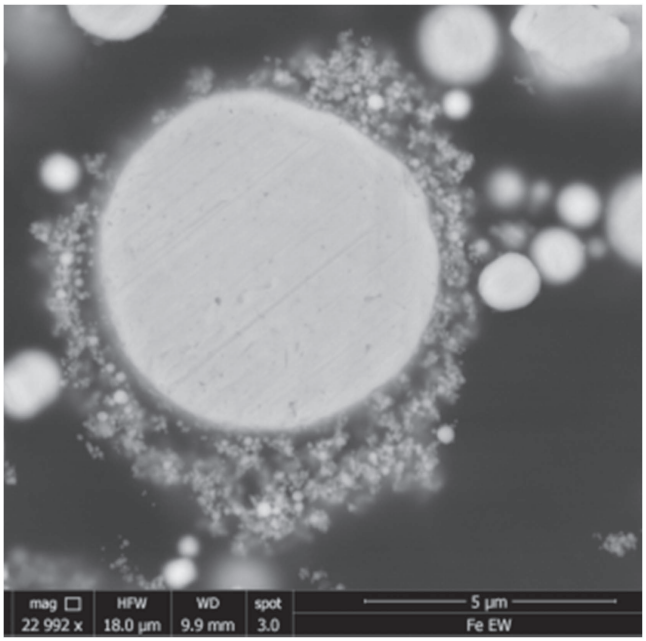

Figure 3. Scanning electron microscopy picture of the bimodal suspensions in a resin. The detail shows a large carbonyl iron microparticle surrounded by iron nanoparticles. Magnetic field density 750 mT.

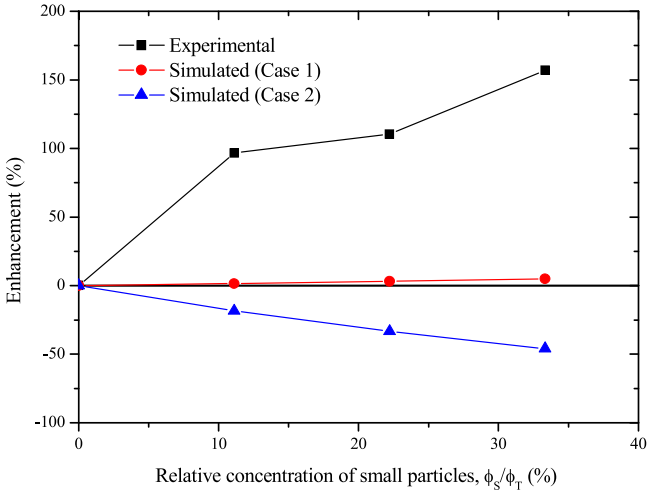

Figure 4. Effective enhancement (%) as a function of the relative concentration of small particles ϕ_S/ϕ_T for a constant total volume fraction of solids of 45 vol% ($\phi_T = 0.45$). The external magnetic field strength is 147 kA m^{-1}.

well captured by numerical simulations suggests that major (interparticle) interactions involved are essentially magnetostatics. These are indeed the only interactions simulated in this work. However, other colloidal forces may influence the experimental data and are not considered in the simulations (e.g. van der Waals, friction, surface charges…). Also, the calculations shown here ground on very strong assumptions; the numerical calculations assume a perfect cubic lattice formed by the larger particles and that the shell of nanoparticles is a continuum of uniform thickness. However, a cubic lattice is never observed at these (large) concentrations

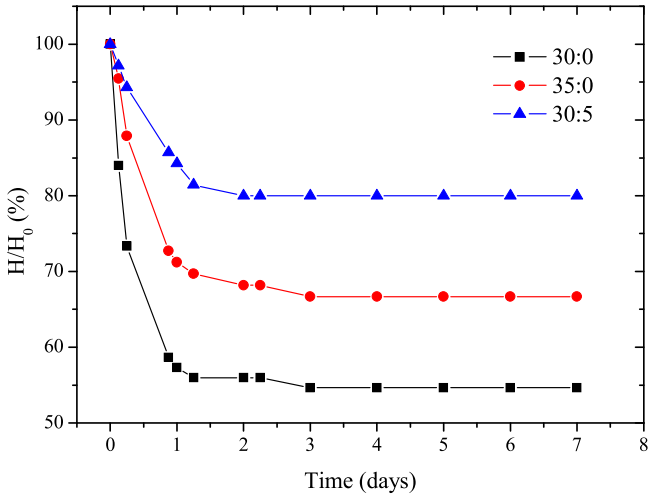

Figure 5. Time evolution of the sedimentation ratio (H/H_0) for conventional MR fluids (30 and 35 vol% large particles) and bimodal MR fluids (30 vol% large + 5 vol% small).

Table 2. Sedimentation characteristics of the bimodal MR fluids (large:small mixtures in vol%).

MR fluid composition (L:S)	Maximum packing fraction (vol%)
30:0	54.9
35:0	52.5
30:5	43.8

and lateral/secondary connections between aggregates appear [25]. Furthermore, a magnetic field gradient is established upon the application of the field around the larger particles and therefore the nanoparticles concentration should be larger in the proximity of the polar regions of the larger particles.

In view of figure 4, it is worth to note that the effective enhancement increases as a result of the fact that the nanoparticles, within the shell structure, have superior magnetic properties than bare microparticles at the magnetic fields investigated (see table 1). Unrealistic results are found again if nanoparticles are well dispersed in the carrier fluid instead of covering the large particles. In this case, as the small size particles concentration increases, the magnetic field within the gap between larger particles is screened due to the increase in the magnetic permeability of the suspension of small particles. In addition, increasing small particles concentration, that is ϕ_S, implies the reduction of ϕ_L, and consequently, the contribution of surrounding large particles is diminished.

The next step was to explore the sedimentation characteristics of the bimodal suspensions compared to the monomodal ones. Results are shown in figure 5 for three suspensions: (i) large particles at a 30 vol% concentration, (ii) large particles at a 35 vol% concentration and (iii) binary mixtures (30 vol% large L + 5 vol% small S). As observed, the sedimentation rate is significantly reduced when microparticles are replaced with nanoparticles. The most tightly packed sediments are always those corresponding to monomodal MR fluids (see table 2). As observed, bimodal suspensions give place to a higher sediment. Such a high sediment is the result of the formation of a not well compacted sediment. This is coherent with the fact that small and large particles are magnetically interacting and do not behave as non-Brownian hard spheres because in this case a particle mixture would give a more efficient packing. The observed slower sedimentation rate is coherent with the presence of more aggregates in suspension [e.g. 16].

Finally, penetration tests demonstrate that sediments formed in bimodal mixtures are also easier to redisperse than monomodal ones. In bimodal suspensions, the mechanical work, for a penetration distance of 40 mm, was of only 1.83 mJ while the torque required for redispersion (at 0.001 rpm) was of only 30 ± 2 μN m. It is worth to note that the monomodal suspensions formed a very compacted cake that could not be penetrated with our rheometer.

Overall, bimodal MR fluids in the single-multidomain limit exhibit a significantly large MR effect (i.e. increase in the on-state yield stress) similar to bimodal suspensions in the range $\sigma_L/\sigma_S \approx 10$ and good stability properties (i.e. reduced settling rate) similar to bimodal suspensions in the range $\sigma_L/\sigma_S \approx 1000$. The key point is the coexistence of two particle populations having an induced and permanent magnetic moment, respectively.

Finite element method simulations results suggest that a crucial point is the superior magnetic characteristics of the nanoparticles if compared to the microparticles. Hence, it can be speculated that the partial substitution of carbonyl iron microparticles by a small amount of very strong magnetic particles (e.g. iron alloys) in the single-multidomain region would provide an even stronger enhancement in the MR response.

Acknowledgments

This work was supported by MAT 2016-78778-R and PCIN 2015-051 projects (FEDER FUNDS and MINECO, Spain). A J F Bombard is grateful to FAPEMIG grants: APQ-01824-17, PEE-00081-16, RED-00144-16, ETC-00043-15, PEP-00231-15, APQ-00463-11 and RDP-00164-10. J R Morillas acknowledges FPU14/01576 fellowship.

ORCID iDs

Juan de Vicente https://orcid.org/0000-0002-2833-2272

References

[1] Foister R T 1997 Magnetorheological fluids *US Patent No.* 5,667,715
[2] Weiss K D, Carlson J D and Nixon A D 2000 Method and magnetorheological fluid formulations for increasing the output of a magnetorheological fluid device *US Patent No.* 6,027,664
[3] See H, Kawai A and Ikazaki F 2002 The effect of mixing particles of different size on the electrorheological response under steady shear flow *Rheol. Acta* **41** 55–60

[4] Trendler A M and Böse H 2004 Influence of particle size on the rheological properties of magnetorheological suspensions *Proc. 9th Int. Conf. on Electrorheological Fluids and Magnetorheological Suspensions* pp 433–9
[5] Ulicny J C, Smith A L, Golden M A, McDermott B L and Chapaton T J 2004 Magnetorheological fluids with an additive package *US Patent No.* 6,824,701
[6] Bombard A J F, Alcantara M R, Knobel M and Volpe P L O 2005 Experimental study of MR suspensions of carbonyl iron powders with different particles sizes *Int. J. Mod. Phys.* B **19** 1332–8
[7] Kittipoomwong D, Klingenberg D J and Ulicny J C 2005 Dynamic yield stress enhancement in bidisperse magnetorheological fluids *J. Rheol.* **49** 1521–38
[8] Gonçalves F D, Koo J H and Ahmadian M 2006 A review of the state of the art in magnetorheological fluid technologies: I. MR fluid and MR fluid models *Shock Vib. Dig.* **38** 203–19
[9] Dodbiba G, Park H S, Okaya K and Fujita T 2008 Investigating magnetorheological properties of a mixture of two types of carbonyl iron powders suspended in an ionic liquid *J. Magn. Magn. Mater.* **320** 1322–7
[10] Ekwebelam C C and See H 2009 Microstructural investigations of the yielding behaviour of bidisperse magnetorheological fluids *Rheol. Acta* **48** 19–32
[11] Li W H and Zhang X Z 2010 A study of the magnetorheological effect of bimodal particle based magnetorheological elastomers *Smart Mater. Struct.* **19** 035002
[12] Rosenfeld N, Wereley N M, Radhakrishnan R and Sudarshan T S 2002 Behavior of magnetorheological fluids utilizing nanopowder iron *Int. J. Mod. Phys.* B **16** 2392–8
[13] Chaudhuri A, Wang G, Wereley N M, Tasovksi V and Radhakrishnan R 2005 Substitution of micron by nanometer scale powders in magnetorheological fluids *Int. J. Mod. Phys.* B **19** 1374–80
[14] López-López M T, de Vicente J, Bossis G, González-Caballero F and Durán J D G 2005 Preparation of stable magnetorheological fluids based on extremely bimodal iron–magnetite suspensions *J. Mater. Res.* **20** 874–81
[15] Wereley N M, Chaudhuri A, Yoo J H, John S, Kotha S, Suggs A, Radhakrishnan R, Love B J and Sudarshan T S 2006 Bidisperse magnetorheological fluids using Fe particles at nanometer and micro scale *J. Intell. Mater. Syst. Struct.* **17** 393–401
[16] Jönkkari I, Isakov M and Syrjälä S 2015 Sedimentation stability and rheological properties of ionic liquid-based bidisperse magnetorheological fluids *J. Intell. Mater. Syst. Struct.* **26** 2256–65
[17] Leong S A N, Mazlan S A, Samin P M, Idris A and Ubaidillah 2016 Performance of bidisperse magnetorheological fluids utilizing superparamagnetic maghemite nanoparticles *AIP Conf. Proc.* **1710** 030050
[18] Cullity B D 1972 *Introduction to Magnetic Materials* (New Jersey: Wiley)
[19] Morillas J R, Bombard A J F and de Vicente J 2016 Preparation and characterization of magnetorheological fluids by dispersion of carbonyl iron microparticles in PAO/1-octanol *Smart Mater. Struct.* **25** 015023
[20] Bombard A J F, Gonçalves F R, Morillas J R and de Vicente J 2014 Magnetorheology of dimorphic magnetorheological fluids based on nanofibers *Smart Mater. Struct.* **23** 125013
[21] Morillas J R and de Vicente J unpublished
[22] Jiles D 1991 *Introduction to Magnetism and Magnetic Materials* (New York: CRC)
[23] Maxwell-Garnett J C 1904 Colours in metal glasses and in metallic films *Phil. Trans. R. Soc.* A **203** 385–420
[24] Ginder J M, Davis L C and Elie L D 1996 Rheology of magnetorheological fluids: models and measurements *Int. J. Mod. Phys.* B **10** 3293–303
[25] de Vicente J 2013 Magnetorheology: a review *Ibero-American J. Rheol.* **1** 1–18